

Supporting Information

Methylation of 2'-Deoxyguanosine by a Free Radical Mechanism

Conor Crean, Nicholas E. Geacintov, and Vladimir Shafirovich

Kinetics of DMSO oxidation by $\text{SO}_4^{\bullet-}$ radicals. Competition of one-electron oxidation of dG to form $\text{dG}(-\text{H})^{\bullet}$ radicals (reaction 3, Table 1) and the one-electron oxidation of DMSO to form $^{\bullet}\text{CH}_3$ radicals:



with the second-order rate constant, k_b can not accurately predict the yields of $\text{dG}(-\text{H})^{\bullet}$ at high concentrations of DMSO. Indeed, the experimental yields of $\text{dG}(-\text{H})^{\bullet}$ radicals at $[\text{DMSO}] \geq 0.8$ mM are systematically higher than those predicted by the equation $[\text{dG}(-\text{H})^{\bullet}]_{t=8\mu\text{s}}/[\text{SO}_4^{\bullet-}]_0 = k_3[\text{dG}]/(k_3[\text{dG}] + k_b[\text{DMSO}])$, where the subscripts “0” and “ $t=8\mu\text{s}$ ” refer to the earliest time points after the actinic laser flash and completion of the formation of $\text{dG}(-\text{H})^{\bullet}$ radicals, respectively (Figure S1)

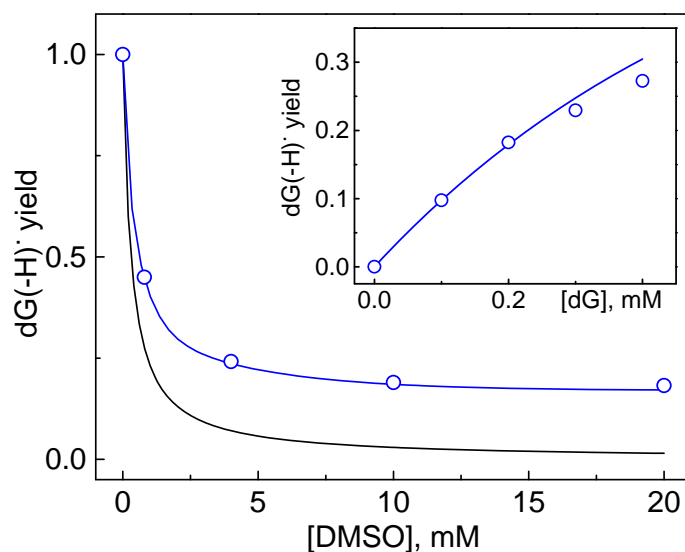


Figure S1. Reaction yields of $\text{dG}(-\text{H})^{\bullet}$ radicals generated by $\text{SO}_4^{\bullet-}$ radicals as a function of DMSO concentration at $[\text{dG}] = 0.2$ mM and $[\text{DMSO}] = 20$ mM (inset). Solid black line shows the $\text{dG}(-\text{H})^{\bullet}$ yields calculated from the equation $[\text{dG}(-\text{H})^{\bullet}]_{t=5\mu\text{s}}/[\text{SO}_4^{\bullet-}]_0 = k_3[\text{dG}]/(k_3[\text{dG}] + k_b[\text{DMSO}])$ at $k_3 =$

$4.1 \times 10^9 \text{ M}^{-1} \text{ s}^{-1}$ (this work and ref.¹) and $k_b = 2.7 \times 10^9 \text{ M}^{-1} \text{ s}^{-1}$ (the previous pulse radiolysis experiments²). The yields of $\text{dG}(-\text{H})^\bullet$ obtained by using the rate constants of reactions 3 – 6 in Table 1 are shown by blue lines.

To address this discrepancy we explored the kinetics of DMSO oxidation by $\text{SO}_4^{\bullet-}$ radicals in a wide range of DMSO concentrations (0.1 – 20 mM). Under these conditions concentrations of the sulfate radicals, $[\text{SO}_4^{\bullet-}] \ll [\text{DMSO}]$ and decay of $\text{SO}_4^{\bullet-}$ radicals can be described by the first-order kinetics with the rate constant, k_a . Figure S2 shows that k_a calculated from the transient absorption profiles of the $\text{SO}_4^{\bullet-}$ decay at 445 and 315 nm, increases linearly as a function of DMSO concentrations at $[\text{DMSO}] < 1 \text{ mM}$.

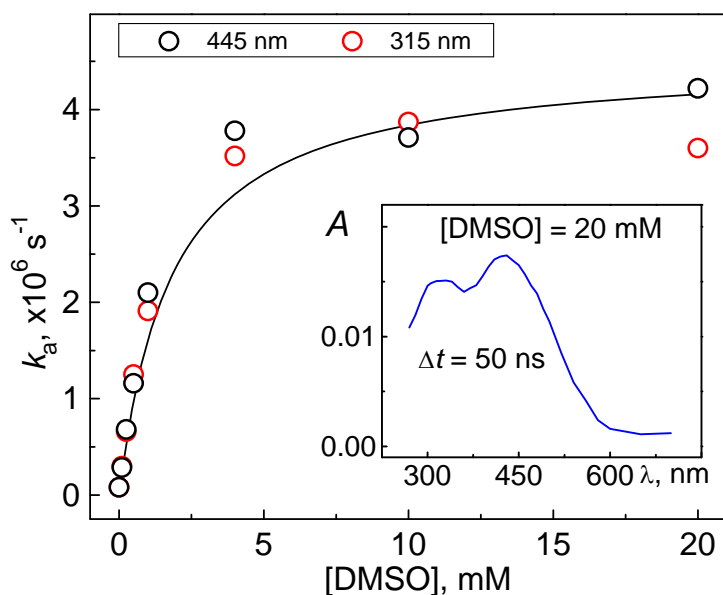


Figure S2. Rate constants, k_a for decay of $\text{SO}_4^{\bullet-}$ radicals at 445 nm (black open circles) and 315 nm (red open circles) as a function of DMSO concentrations. Fitting the equation $k_a = k_5 K_4 [\text{DMSO}] / (1 + K_4 [\text{DMSO}])$, where $K_4 = k_4 / k_{-4}$ is the equilibrium constant of the $[\text{SO}_4^{\bullet-} \dots \text{DMSO}]$ complex formation, to the experimental data points is shown by a solid black line. Inset shows the transient absorption spectrum recorded at 50 ns after an actinic laser flash.

At [DMSO] > 1 mM the k_a dependence significantly deviates from a linear one and at [DMSO] > 5 mM the value of k_a attains a value, which only slightly depends on [DMSO]. This non-linear behavior of the k_a vs [DMSO] plot can be considered as indication for formation of the [SO₄^{•-}...DMSO] complex. The spectrum of this complex recorded at 50 ns after an actinic laser flash at [DMSO] = 20 mM (inset in Figure S2) is very close to the spectrum of SO₄^{•-} radicals shown in Figure 1. This spectrum significantly differs from the spectra of DMSO^{•+} obtained at pH 4, where these radical cations are stable on a microsecond time scale and exhibit a broad absorption band at 300 nm with a greater extinction coefficient² of $\sim 4 \times 10^3 \text{ M}^{-1} \text{ cm}^{-1}$ than $\sim 1.2 \times 10^3 \text{ M}^{-1} \text{ cm}^{-1}$ in the case of SO₄^{•-} radicals. The absence of the DMSO^{•+} absorption band in the spectrum of the [SO₄^{•-}...DMSO] complex recorded at pH 7.4 (inset in Figure S2) suggests that fragmentation of DMSO^{•+} with formation of [•]CH₃ radicals occurs in not rate-determining step and decay of the [SO₄^{•-}...DMSO] complex is controlled by electron transfer from DMSO to SO₄^{•-}.

Fitting the equation $k_a = k_5 K_4 [\text{DMSO}] / (1 + K_4 [\text{DMSO}])$ to the experimental data points (Figure S2) allows to determine the equilibrium constant of the [SO₄^{•-}...DMSO] complex formation, $K_4 = k_4 / k_{-4} = 480 \text{ M}^{-1}$ and the rate constant of the adduct decay, $k_5 = 4.2 \times 10^6 \text{ s}^{-1}$ (Table 1) to form [•]CH₃ radicals. At $K_4 [\text{DMSO}] < 1$ oxidation of DMSO by SO₄^{•-} radicals follows second order kinetics with $k_b = k_5 K_4 = 2 \times 10^9 \text{ M}^{-1} \text{ s}^{-1}$, which is in a reasonable agreement with $k_b = 2.7 \times 10^9 \text{ M}^{-1} \text{ s}^{-1}$ obtained in the previous pulse radiolysis experiments.² Since at high [DMSO] the equilibration between SO₄^{•-} radicals, DMSO, and the complex is very fast, we suggested that the complex is controlled by diffusion of the reaction partners ($k_4 = 1 \times 10^{10} \text{ M}^{-1} \text{ s}^{-1}$) that gives $k_{-4} = 2.1 \times 10^7 \text{ s}^{-1}$ for the adduct dissociation (Table 1).

In the complex SO₄^{•-} radical remains a strong oxidant that can oxidize dG to contribute in formation of dG(-H)[•] (reaction 6). This reaction with the rate constant, $k_6 = 3.8 \times 10^9 \text{ M}^{-1} \text{ s}^{-1}$ (Table 1) can explain the experimental yields of dG(-H)[•] in all range of [DMSO] (Figure S2).

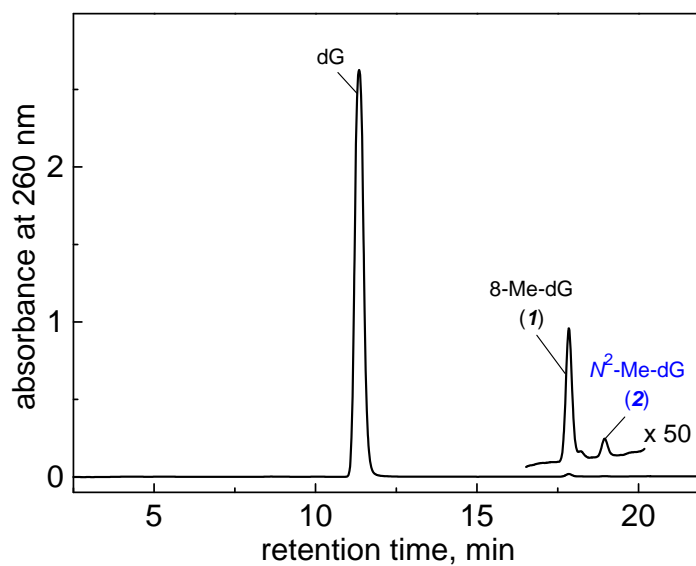


Figure S3. End-products generated by photolysis of 0.1 mM methylcob(III)alamin (0.1 μ mole) in the presence of 1 mM dG (1 μ mole) in deoxygenated 10mM phosphate buffer sample solutions (1 ml) using 340 – 390 nm steady-state irradiation (~ 100 mW/cm²) from a 100 W Xe arc lamp for 10 min. Reversed-phase HPLC elution conditions (detection of products at 260 nm): 1 – 40% gradient of methanol in 20 mM sodium phosphate buffer (pH 7) over 60 min.

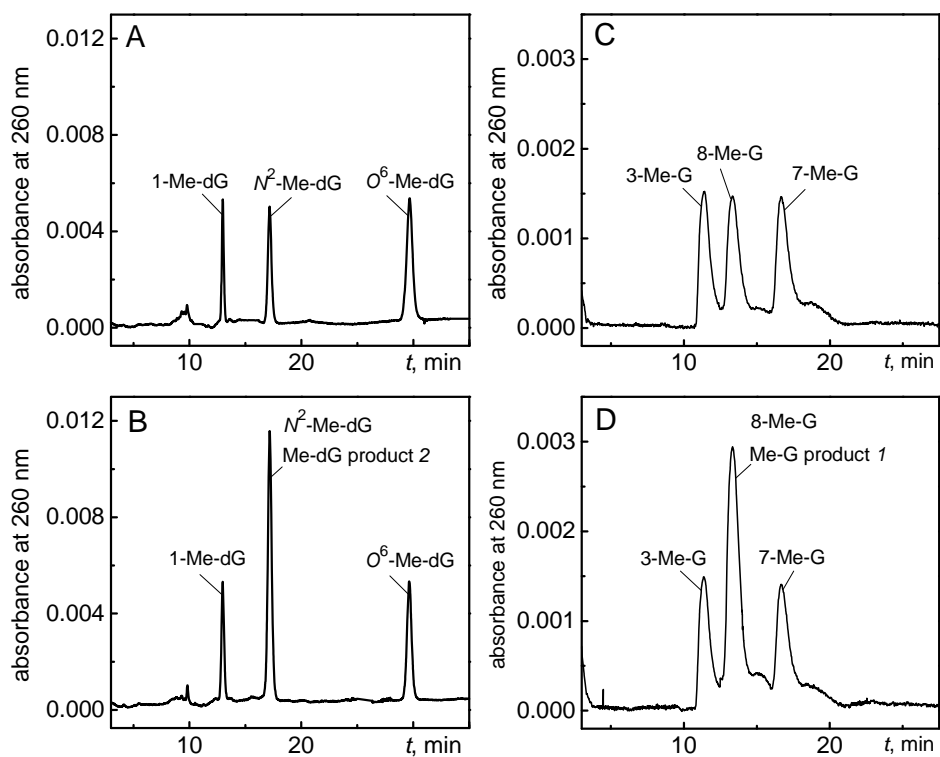


Figure S4. Reversed-phase HPLC analysis of the Me-dG product **2** (A, B) and Me-G product **1** (C, D). HPLC elution conditions (detection of products at 260 nm): Panels A and B: 0 – 30% gradient of methanol in 20 mM ammonium acetate over 60 min; the Me-dG product **2** co-elutes with N^2 -Me-dG at 17.1 min. Panels C and D: isocratic elution with 99% H_2O : 1% methanol ; the Me-G product **1** co-elutes with 8-Me-G at 13.3 min.

Positive product ion spectra of methyl-2'-deoxyguanosines. In order to obtain more direct structural information on the positions of the methyl groups, LC-MS/MS methods were employed to investigate the distributions of daughter ions generated by the extensive fragmentation of the aglycone ions, $[\text{BH}_2]^+$, derived from the detachment of the sugar residues from the molecular ions. The positive product ion spectra of the unlabeled (natural ^{14}N -isotopes) and uniformly ^{15}N -labeled samples of 8-Me-dG and N^2 -Me-dG derived from the combination of the $\text{dG}(-\text{H})^\bullet$ and $^\bullet\text{CH}_3$ radicals (Figure S5).

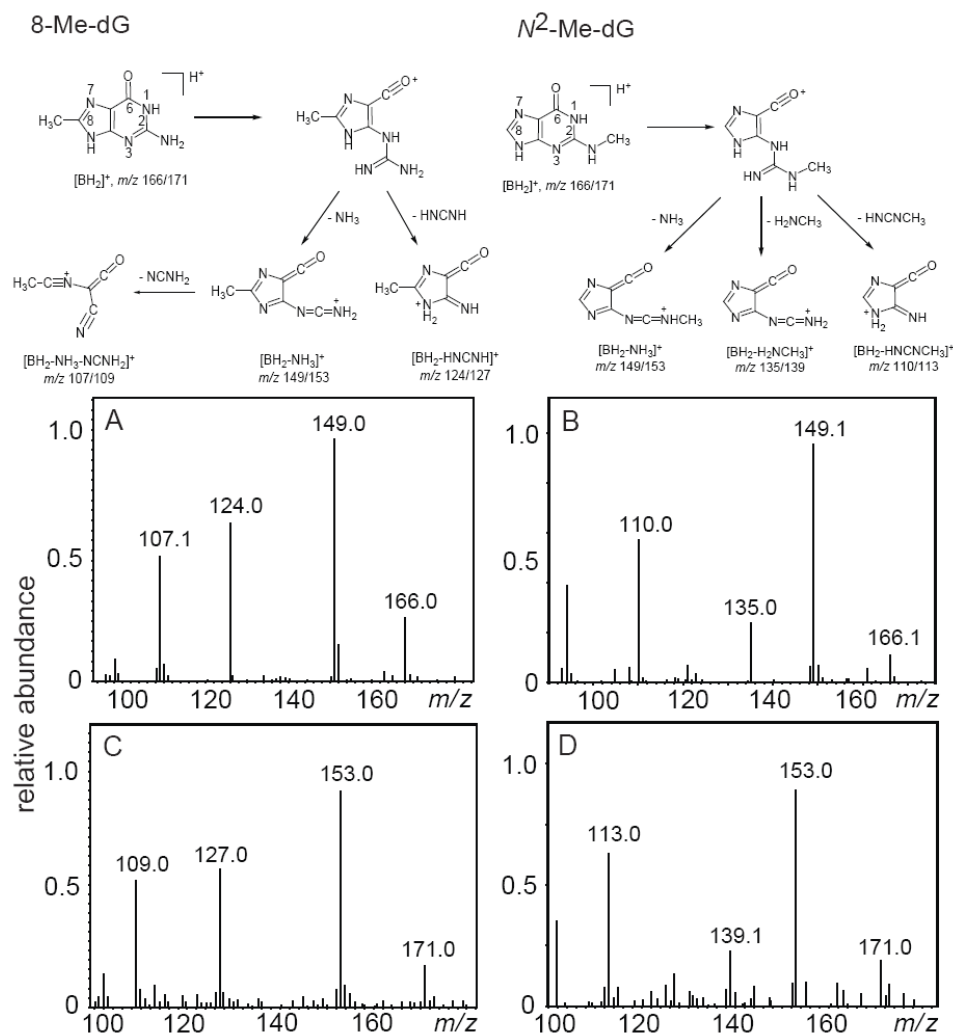


Figure S5. Positive product ion spectra of the unlabeled (natural ^{14}N -isotopes, Panels A and B) and uniformly labeled (^{15}N -isotopes, Panels C and D) 8-methyl-dG (Panels A and C) and N^2 -methyl-dG (Panels B and C) isolated from the irradiated solutions as shown in Figure 5. Fragmentation pathways of the aglycone ions, $[\text{BH}_2]^+$ triggered by the opening of the pyrimidine ring³ are shown at the top of this Figure.

In these spectra, the differences in the masses of the ions of ^{14}N -Me-dG and ^{15}N -Me-dG products yield the number of nitrogen atoms in these ions.

We found that the fragmentation of the $[\text{BH}_2]^+$ ions can be rationalized in terms of the mechanism proposed by Gregson and McCloskey for guanine.³ According to this mechanism, the fragmentation of the $[\text{BH}_2]^+$ ions is triggered by the initial opening of the pyrimidine ring followed by two principal pathways validated by ^{15}N -labeling: (i) expulsion of ammonia (NH_3) or methylamine (H_2NCH_3), and (ii) expulsion of the CH_2N_2 fragment via two tautomeric forms (cyanamide, NCNH_2 , or carbodiimide, HNCNH), or the $\text{C}_2\text{H}_4\text{N}_2$ fragment in the form of the *N*-methylcarbodiimide (HNCNCH_3). The first pathway results in the formation of the $[\text{BH}_2\text{-NH}_3]^+$ ion at m/z 149 detected in the spectra of all methylguanine products (Figures S5A, S5B and S6 – S11), and the $[\text{BH}_2\text{-H}_2\text{NCH}_3]^+$ ion at m/z 135 observed in the case of N^2 -Me-G (Figures S5B and S7), but not in the case of 8-Me-G (Figures S5A and S11). In the case of 8-Me-G the second pathway associated with the excision of the CH_2N_2 fragment results in the formation of the $[\text{BH}_2\text{-HNCNH}]^+$ ion at m/z 124 and the $[\text{BH}_2\text{-NH}_3\text{-NCNH}_2]^+$ ion at m/z 107, respectively (Figures S5A and S11). These ions are not observed in the N^2 -Me-G spectrum, because in this compound, the exocyclic NH_2 group is methylated and the second pathway results in the expulsion of *N*-methylcarbodiimide (HNCNCH_3) to form the $[\text{BH}_2\text{-HNCNCH}_3]^+$ ion at m/z 110 (Figures S5B and S7). Thus, analysis of the fragment ion distributions allows a straightforward differentiation of 8-Me-G and N^2 -Me-G in which different rings are methylated (purine in 8-Me-G and pyrimidine in N^2 -Me-G). However, the differentiation of N^2 -Me-G and 1-Me-G is not feasible because, after the initial pyrimidine ring opening (Figures S5B, S6 and S7), the N1 and N^2 atoms become undistinguishable.³

Differentiation between 8-Me-G (Figures S5A and S11) and 7-Me-G (Figure S10) is also not possible, because the positive ion spectra of these isomers are practically the same. Although 3-Me-G does not show any ion products with m/z 124, it exhibits an ion at m/z 107 (Figure S8) that does not allow for a direct identification of this product in the presence of 7-Me-G and 8-Me-G. In turn, O^6 -Me-dG (Figure S9) can be differentiated from 1-Me-G and N^2 -Me-G (Figures S6 and S7) by the appearance of the marker ion at m/z 134. The series of daughter ions detected at m/z 166, 149, 134 and 110 in the case of

O^6 -CH₃-dG is altered to ions detected at m/z 169, 152, 134 and 110 in the case of O^6 -CD₃-dG with deuterium atoms in the methyl group.⁴ According to these results, the ion at m/z 134 is formed via expulsion of the CH₃/CD₃ group from the [BH₂-NH₃]⁺ ion at m/z 149 that allows for a differentiation of O^6 -CH₃-dG from other methyl guanines (Figures S6 – S11). Thus, analysis of the fragmentation patterns provides a direct differentiation of O^6 -Me-dG and of other methylguanines into two groups: (i) 7-Me-G, 8-Me-G, and 3-Me-G, and (ii) 1-Me-G and N^2 -Me-G.

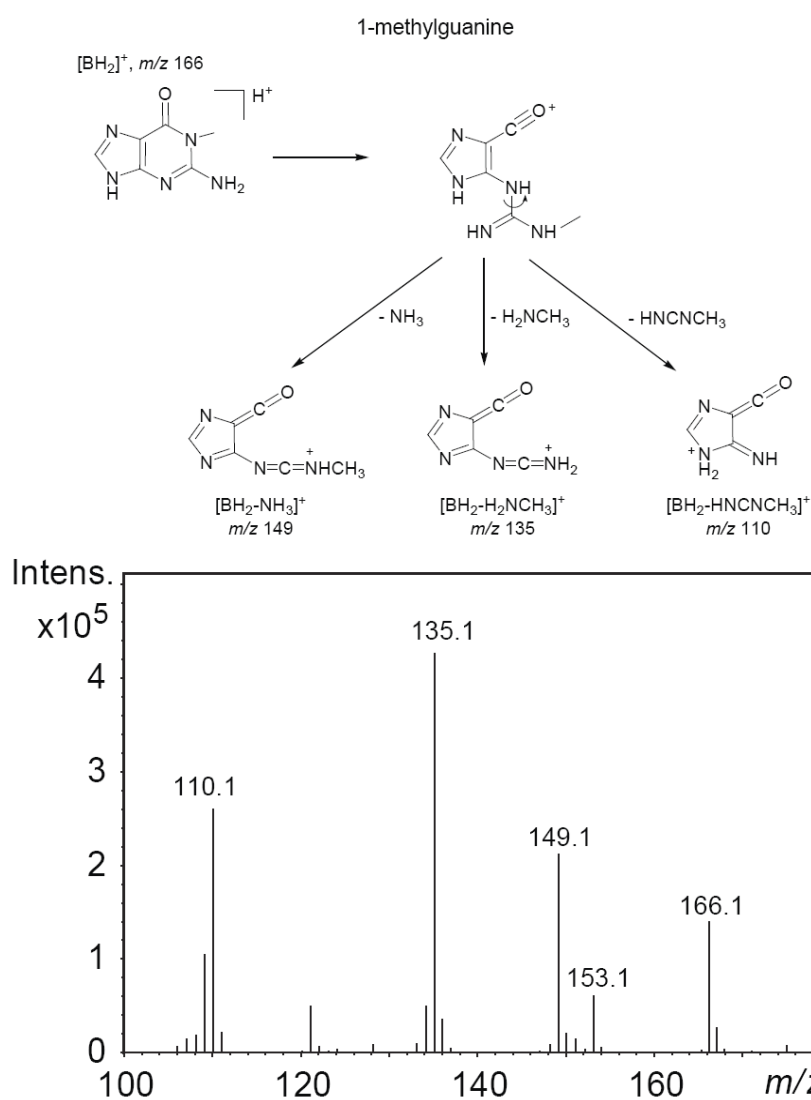


Figure S6. Positive product ion spectra of 1-methylguanine.

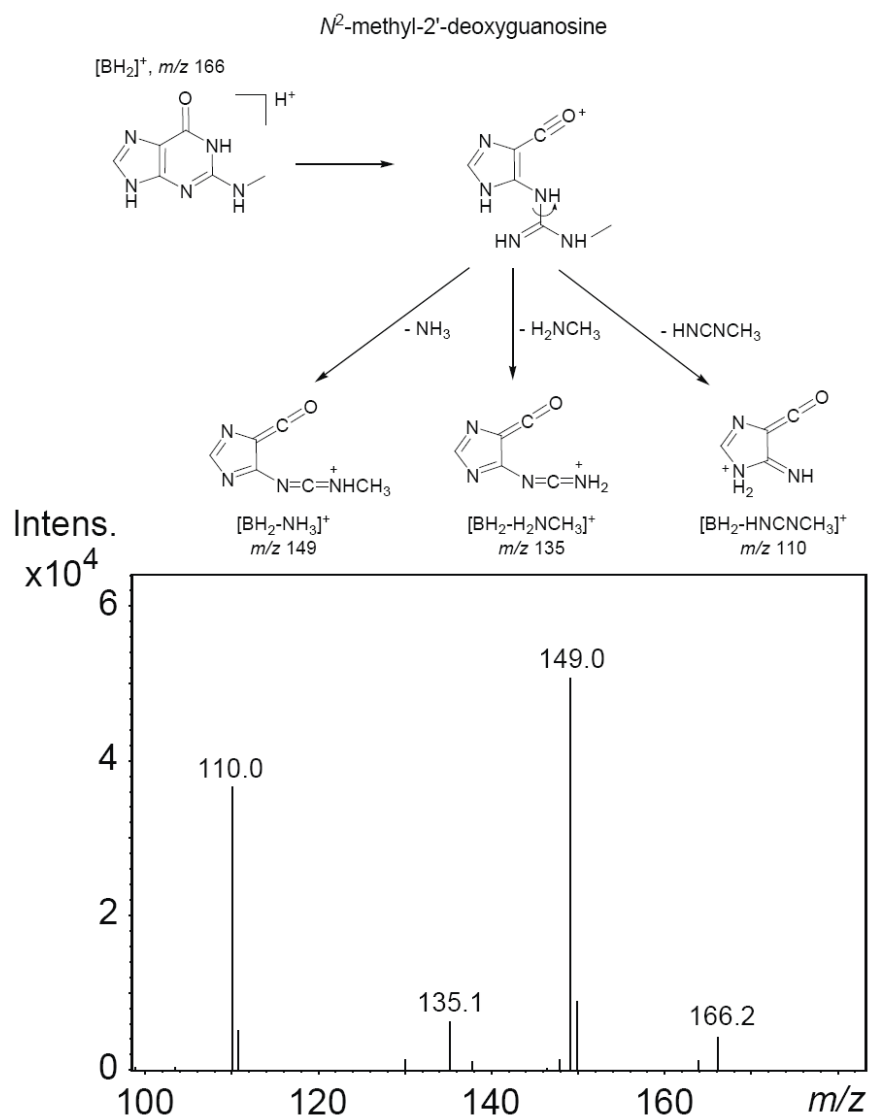


Figure S7. Positive product ion spectra of *N*²-methyl-dG.

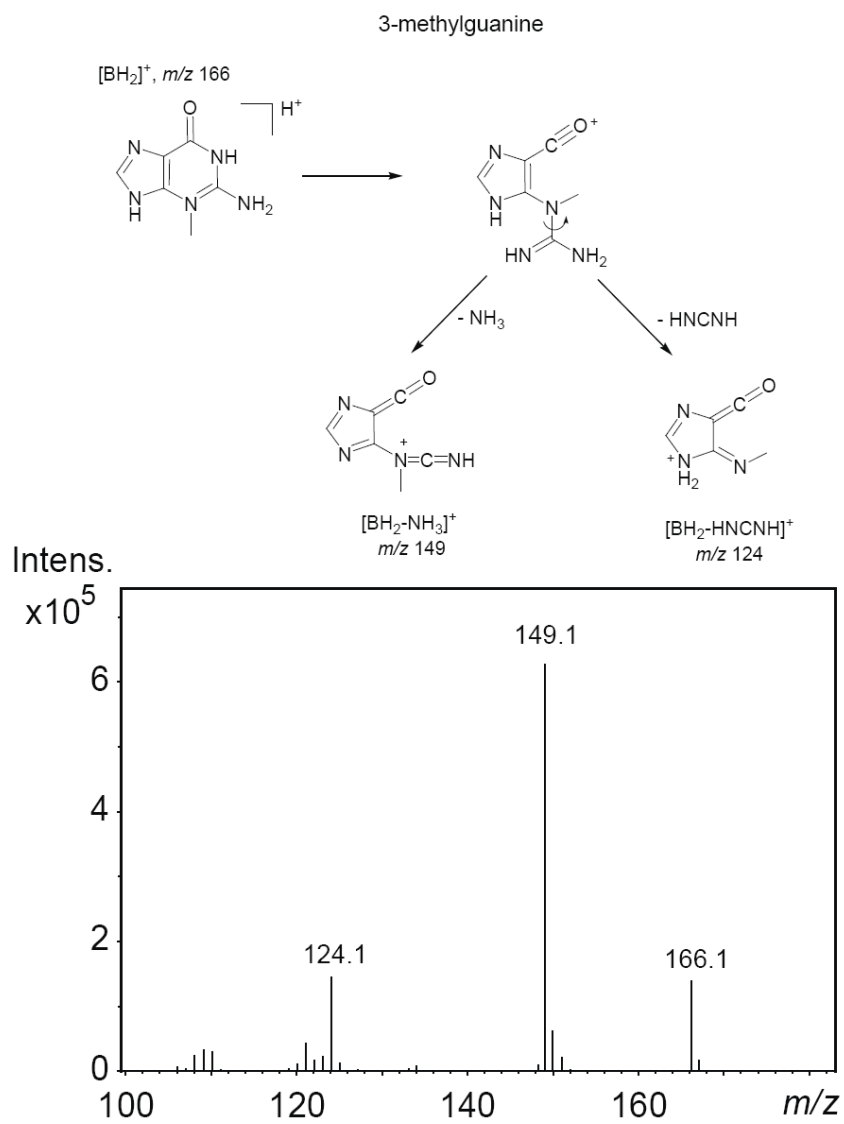


Figure S8. Positive product ion spectra of 3-methylguanine.

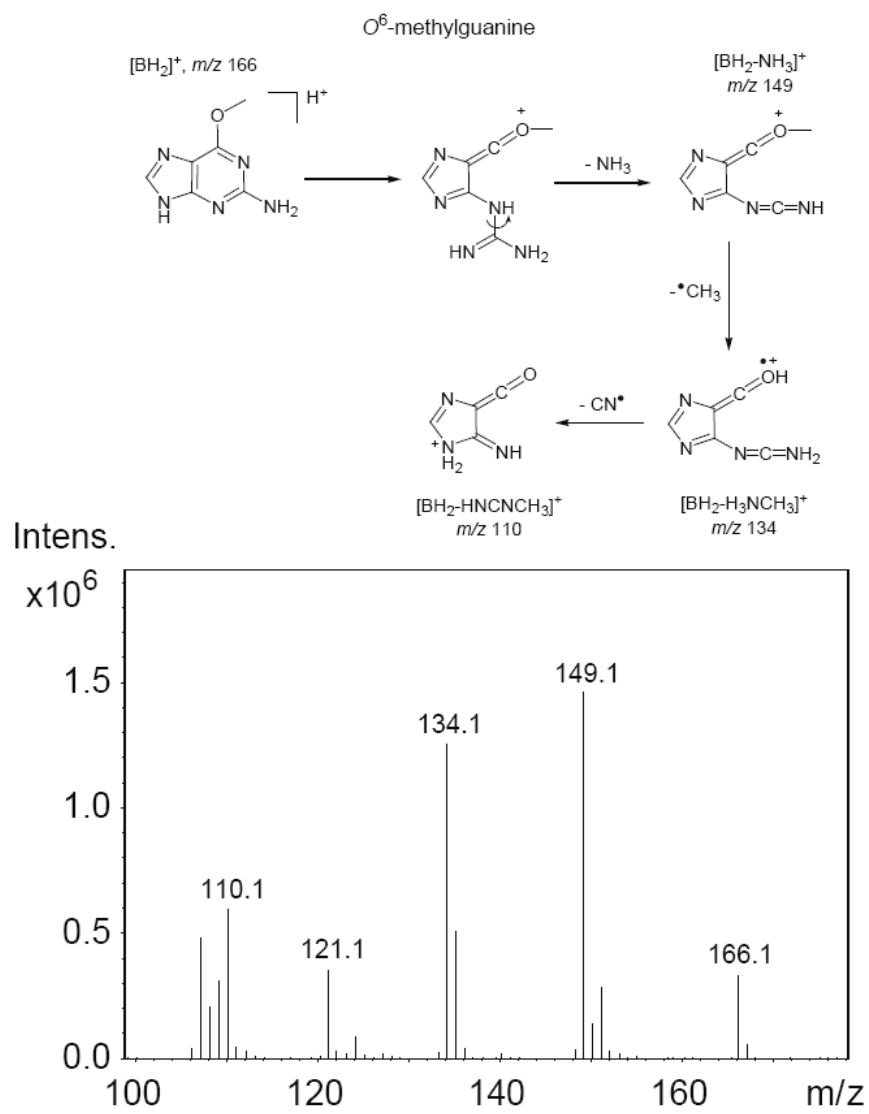


Figure S9. Positive product ion spectra of *O*⁶-methyl-dG.

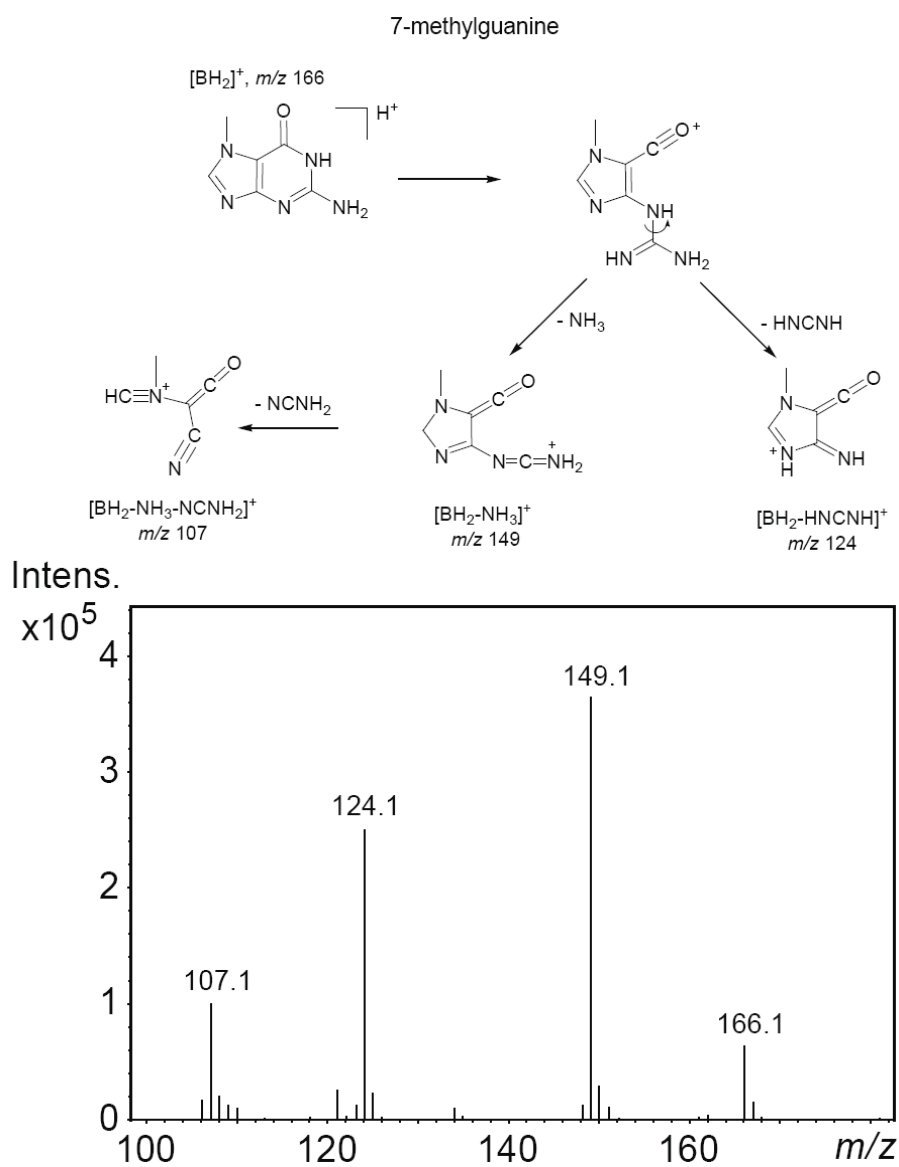


Figure S10. Positive product ion spectra of 7-methylguanine.

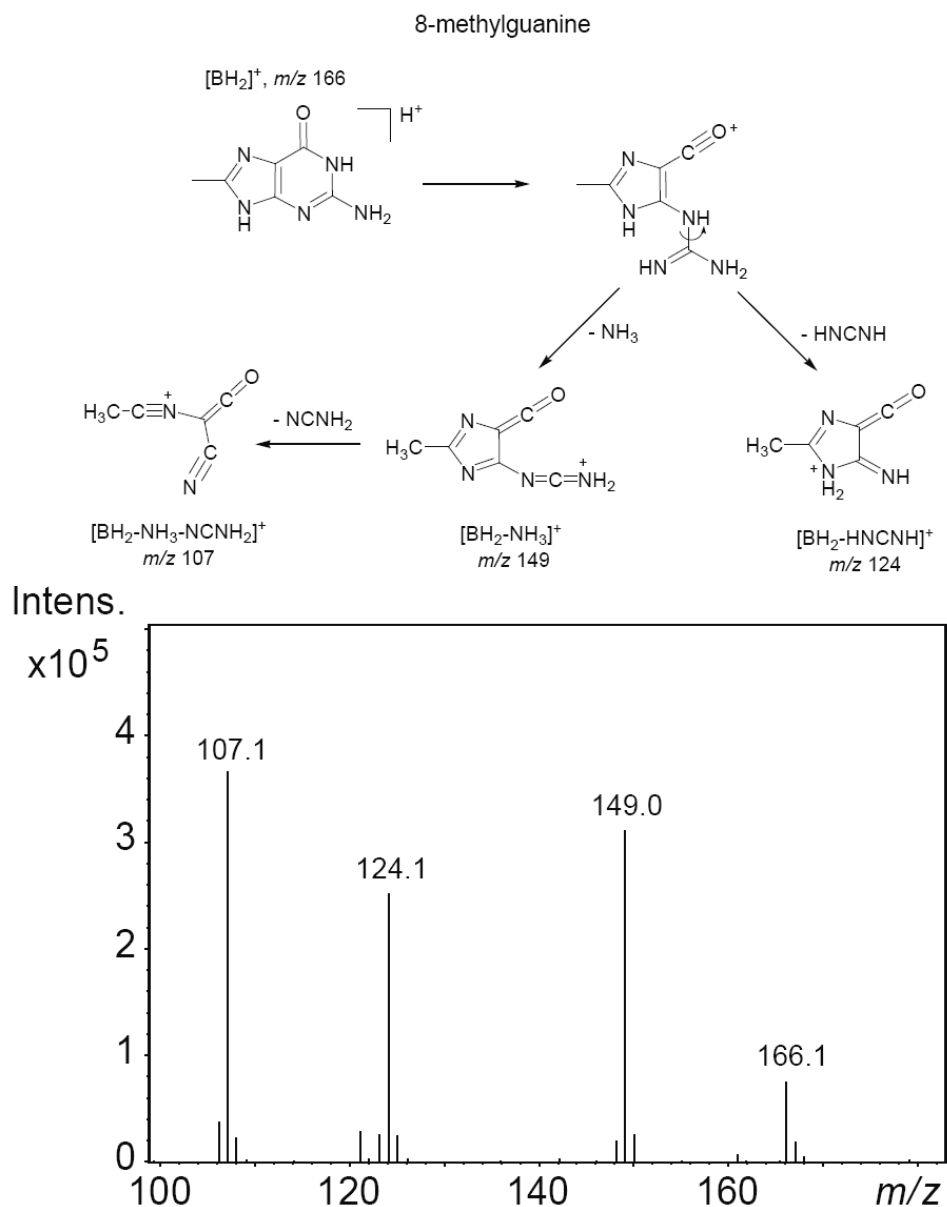


Figure S11. Positive product ion spectra of 8-methylguanine.

References

- (1) Candeias, L. P.; Steenken, S. *J. Am. Chem. Soc.* **1989**, *111*, 1094-1099.
- (2) Kishore, K.; Asmus, K.-D. *J. Chem. Soc. Perkin Trans. 2* **1989**, 2079-2084.
- (3) Gregson, J. M.; McCloskey, J. A. *Int. J. Mass Spectrom.* **1997**, *165/166*, 475-485.
- (4) Zhang, F.; Bartels, M. J.; Pottenger, L. H.; Gollapudi, B. B.; Schisler, M. R. *J. Chromatogr. B* **2006**, *833*, 141-148.